Toxicology Letters 183 (2008) 72–80

Contents lists available at ScienceDirect

Toxicology Letters

journal homepage: www.elsevier.com/locate/toxlet

Potential neurological lesion after nasal instillation of TiO_2 nanoparticles in the anatase and rutile crystal phases

Jiangxue Wang[a,b], Chunying Chen[a,b,*], Ying Liu[a,b], Fang Jiao[a,b], Wei Li[a,b], Fang Lao[a,b], Yufeng Li[a,b], Bai Li[a,b], Cuicui Ge[a,b], Guoqiang Zhou[a,b], Yuxi Gao[a,b], Yuliang Zhao[a,b,**], Zhifang Chai[a,b]

[a] *Laboratory for Bio-Environmental Effects of Nanomaterials and Nanosafety and Key Lab of Nuclear Analytical Techniques, Institute of High Energy Physics, Chinese Academy of Sciences, Beijing 100049, PR China*
[b] *National Center for Nanoscience and Technology, Beijing 100190, PR China*

ARTICLE INFO

Article history:
Received 27 June 2008
Received in revised form
27 September 2008
Accepted 2 October 2008
Available online 17 October 2008

Keywords:
TiO_2 nanomaterials
Neurotoxicology
Redox status
Protein oxidation
Lipid peroxidation
GFAP expression

ABSTRACT

Nanoscale titanium dioxide (TiO_2) is massively produced and widely used in living environment, which hence make the potential risk to human health. Central nervous system (CNS) is the potential susceptible target of inhaled nanoparticles, but the studies on this aspect are limited so far. We report the accumulation and toxicity results in vivo of two crystalline phases of TiO_2 nanoparticles (80 nm, rutile and 155 nm, anatase; purity >99%). The female mice were intranasally instilled with 500 μg of TiO_2 nanoparticles suspension every other day for 30 days. Synchrotron radiation X-ray fluorescence analysis (SRXRF) and inductively coupled plasma mass spectrometry (ICP–MS) were used to determine the contents of titanium in murine brain. Then, the pathological examination of brain tissue, oxidative stress-mediated responses, and levels of neurochemicals in the brain of exposed mice were also analyzed. The obvious morphological changes of hippocampal neurons and increased GFAP-positive astrocytes in the CA4 region were observed, which were in good agreements with higher Ti contents in the hippocampus region. Oxidative stress occurred obviously in whole brain of exposed mice such as lipid peroxidation, protein oxidation and increased activities of catalase, as well as the excessive release of glutamic acid and nitric oxide. These findings indicate anatase TiO_2 nanoparticles exhibited higher concern on some tested biological effects. To summarize, results provided the preliminary evidence that nasal instilled TiO_2 nanoparticles could be translocated into the central nervous system and cause potential lesion of brain, and the hippocampus would be the main target within brain.

1. Introduction

Nanoscale TiO_2 particles (diameter <100 nm) are now massively produced and widely used for paint, printing ink, rubber, paper, cosmetics, car materials, cleaning air, and decomposing organic matters in wastewater because of its inherent advantages of anticorrosion and nanoscale-enhanced photocatalysis. In 2006, International agency for research on cancer (IARC) classified pigment-grade TiO_2 as possibly carcinogenic to human beings (Group 2B) (Baan et al., 2006). The nanoparticle is small enough and much less than the diameter of common cells or red blood cells. Thus, it has an opportunity to enter into human body during the production, transportation, storage, and consumption. However, the influences of TiO_2 nanoparticles on human health are quite uncertain and less known.

Recently, the potential impacts of nanomaterials on human and the environment have attracted great attention of scientists, industries and regulatory issues of governments (Colvin, 2003; Donaldson et al., 2004; Nel et al., 2006; Oberdörster et al., 2005). Some pioneering work has explored the adverse health effects of ultrafine and fine TiO_2 particles. They revealed the increased neutrophils and phagocytes in bronchoalveolar lavage (BAL) fluid and lactate dehydrogenase (LDH) leakage in the lung of rats and mice after exposure to TiO_2 particles (Bermudez et al., 2002, 2004; Oberdörster et al., 1992), the sunlight-illuminated TiO_2 catalyzed DNA damage *in vitro* (Wamer et al., 1997). In our previous study, the liver and kidneys of mice were slightly affected by TiO_2 nanoparti-

* Corresponding author at: Laboratory for Bio-Environmental Effects of Nanomaterials and Nanosafety, National Center for Nanoscience and Technology (NCNST), No. 11, 1st North Street, Zhongguancun, Beijing 100080, PR China. Tel.: +86 10 82545560; fax: +86 10 62656765.
** Corresponding author at: Laboratory for Bio-Environmental Effects of Nanomaterials and Nanosafety, National Center for Nanoscience and Technology (NCNST) and Institute of High Energy Physics (IHEP), Chinese Academy of Sciences, Yuquanlu 19B, Beijing 100049, PR China. Tel.: +86 10 88233191; fax: +86 10 88233191.
E-mail addresses: chenchy@nanoctr.cn (C. Chen), zhaoyuliang@ihep.ac.cn (Y. Zhao).

0378-4274/$ – see front matter © 2008 Elsevier Ireland Ltd. All rights reserved.
doi:10.1016/j.toxlet.2008.10.001

cles after the acute oral exposure at a fixed large dose of 5 g/kg body weight (Wang et al., 2007b). However, the potential translocation of different types of nanoparticles into the central nervous system (CNS) via olfactory pathway has been reported (Nel et al., 2006; Oberdörster and Utell, 2002). Results showed the increased Mn content in the rat brain after instillation of manganese phosphate and sulfate (Normandin et al., 2004), and an increase of ^{13}C concentration in the olfactory bulb, cerebrum and cerebellum of rat brain exposed to carbon particles (Oberdörster et al., 2004). Severe damage to brain was induced when largemouth bass lived in the water containing 500 ppb fullerene (Oberdörster, 2004). Moreover, it was found that nanoscale TiO_2 (P25) particles could stimulate brain microglia to produce reactive oxygen species (ROS) through the oxidative burst, and interfere with mitochondrial energy production *in vitro* (Long et al., 2006). However, what kind of pathological and physiological changes will happen after nanoparticles reaching the brain, which is an important issue being still unknown so far.

The properties of small size and large surface area render nanoparticles high reactivity to generate ROS, which is involved in the lung injury observed from the clinical and experimental studies (Donaldson et al., 2004; Nel et al., 2006; Oberdörster et al., 2005; Yamamoto et al., 2006). Because there are many inflammatory cells in the airways of lung including neutrophils, monocytes, and alveolar macrophages, the oxidative stress is induced and is cell-type specific when the ambient air particle or ultrafine particles (TiO_2, carbon nanotubes and carbon black) are inhaled or instilled. Nanoscale TiO_2 particles are easily photo-activated to produce free radicals, such as hydroxyl radical to induce the cytoskeletal dysfunctions of macrophages (Rahman et al., 2002). After exposure to TiO_2 nanoparticles, Syrian hamster embryo cells showed the micronuclei and apoptosis, and brain microglia cells could release H_2O_2 and O^{2-} (Long et al., 2006). Because the brain is rich in polyunsaturated lipids and sensitive to ROS, it is important to know that what would happen if TiO_2 nanoparticles entered the brain through the olfactory pathway or metabolic pathway.

Another important issue is whether or not the deposited nanoparticles would affect the neural cells which relates to the function of brain. Among the neural cells, astrocytes, constituting the majority of resident glial cells, are present in almost 10 times more in number than neurons in normal adult brain. Glial fibrillary acidic protein (GFAP) is an intermediate filament (IF) protein that is found in glial cells such as astrocytes. GFAP is often considered as the specific biomarkers for the activation of astrocytes. Astrocytes perform many functions, including biochemical support of endothelial cells which form the blood–brain barrier, the provision of nutrients to the nervous tissue, and a principal role in the repair and scarring process in the brain.

Therefore, in this study, after intranasal instilling two crystalline phases of TiO_2 nanoparticles (80 nm, rutile and 155 nm, anatase; purity >99%), we firstly aim to observe Ti micro-distribution and the morphological changes of neurons in the brain of mice, as well as the changes for astrocytes. Secondly, in order to better understand the neurotoxicological mechanism of TiO_2 nanoparticles, the oxidative stress-mediated responses (including lipid and protein oxidation), and the influences on neurochemicals including acetylcholinesterase activity (AChE), and levels of glutamic acid (Glu), and nitric oxide (NO), were further analyzed.

2. Materials and methods

2.1. Materials

Nano-sized TiO_2 particles without any coating were purchased from Hangzhou Dayang Nanotechnology Co. Ltd. (80 nm) and Zhonglian Chemical Medicine Co.

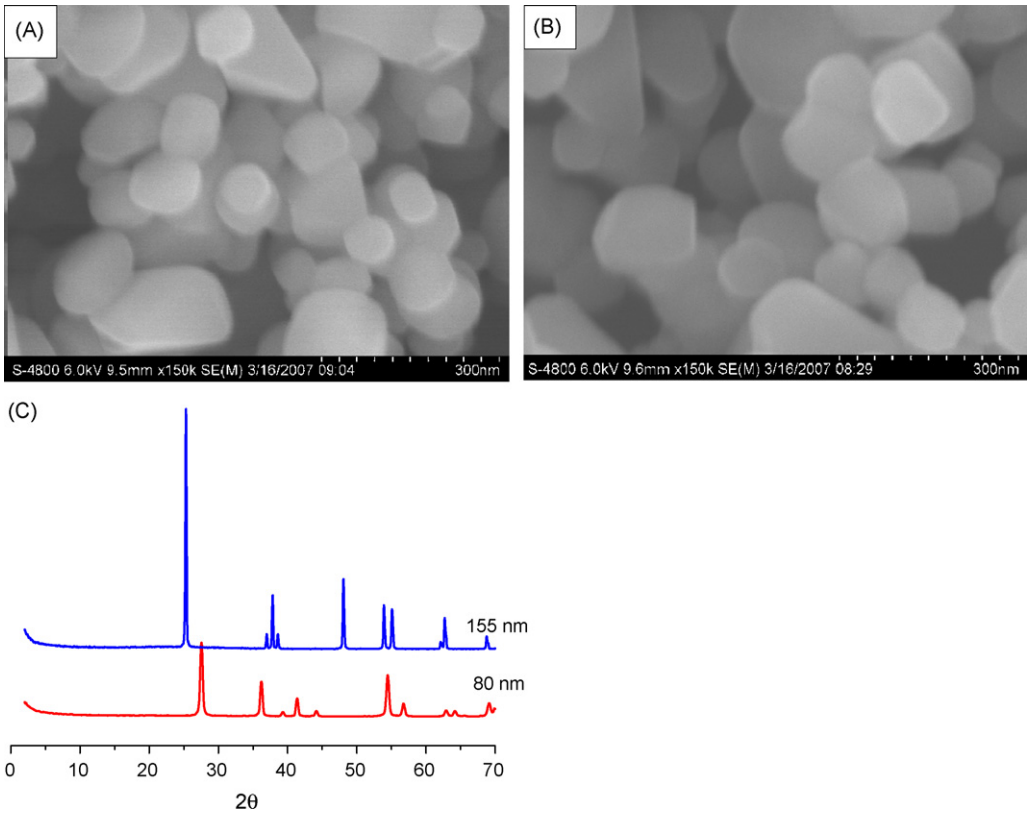

Fig. 1. SEM micrographs of different-sized TiO_2 particles (A) 80 nm; (B) 155 nm in water suspensions and X-ray diffraction pattern of TiO_2 nanoparticles (C). The tested TiO_2 particles of 80 nm are rutile profile and those of 155 nm are anatase profile.

Table 1
Characterization of TiO_2 nanoparticles.

Parameters	Crystalline phase	Purity (Ti)	Particle size and distribution in water (nm)	Surface area (m^2/g)	Single point total pore volume at $P/P_0 = 0.99$ (m^2/g)	Average pore diameter (4V/A by BET) (nm)
80 nm TiO_2	100% Rutile	>99.9%	71.43 ± 23.53	22.69	0.09	16.60
155 nm TiO_2	100% Anatase	>99.9%	154.98 ± 32.98	10.47	0.04	16.77

Note: P: pressure for the absorbate; P_0: saturation vapor pressure for the absorbate.

(155 nm). Their purities (>99%) and sizes were well characterized as same as described in our previous publications (Wang et al., 2007a, 2007b). In addition, we further measured the size of TiO_2 nanoparticles in water profile by scanning electron microscopy (Hitachi S-4800 SEM) (Fig. 1). Surface properties for TiO_2 nanoparticles such as surface area, average pore diameter and pore volume were determined under ASAP 2010 apparatus (Micromeritics, USA) by N_2 absorption at 77.3 K. Crystal profile and structure state of TiO_2 nanoparticles were also characterized by wide-angle X-ray diffractometry (Rigaku D/max 2400, Japan). The 80 nm TiO_2 particles are rutile profile with the average size of 71.43 ± 23.53 nm, and the 155 nm one is anatase profile with the average size of 154.98 ± 32.98 nm (Table 1). Their surface areas increase with the reduction of particle size. But their pore diameters are almost the same, which are 16.60 and 16.77 nm for the 80 and 155 nm TiO_2 nanoparticles, respectively.

A Milli-Q water system (Millipore, Bedford, MA, USA) was used to prepare the ultrapure water. Bovine serum albumin, phenylmethanesulfonyl fluoride (PMSF) and coomassie brilliant blue G-250 were purchased from Sigma Co. (St. Louis, Mo., USA). All of other reagents were at least of analytical grade.

2.2. Animals

CD-1(ICR) female mice (Beijing Vitalriver Experimental Animal Technology Co. Ltd., body weights of 21 ± 2 g) were housed in groups in stainless steel cages. The standard conditions (20 ± 2 °C room temperature, 60 ± 10% relative humidity) were maintained with a 12-h light/dark cycle for mice. Distilled water and sterilized food for mice were available *ad libitum*. All procedures used in this experiment were compliant with the local ethics committee. Animals were acclimated to this environment for 5 days prior to treatment.

The animals were randomly divided into three groups: the control, 80 nm, and 155 nm groups. TiO_2 nanoparticles with no further treatment were dispersed in Milli-Q water and the suspensions were ultrasonicated for 15–20 min to keep the maximum dispersed state. Then the suspensions were vortexed for 2–3 min between the intervals of nasal instillation for different mice. CD-1(ICR) female mice were instilled vehicle or nanoparticles (500 μg per mice) intranasally by a microsyringe every other day. The equal volume of Milli-Q water was given to the control mice. The mice were observed for mortality, body weight, and other clinical signs. During the administration, no other abnormal daily activity was observed for all mice except occasional irritation within 1 h post-exposure.

After the last instilling (i.e. 15 times later), animals were anaesthetized by ether at 24 h post-exposure (on day 30). Mice were perfused with saline solution and then each brain was carefully removed from the skull, washed with Milli-Q water, then the meninges were carefully removed. Three murine brains per group were used to detect Ti-element distribution and observe histopathological changes using frozed sections in the hexane at −70 °C. Then the remaining brain tissues of 12 mice per group were used for determination of biochemical indexes described as below. For quantitatively determining the titanium contents in sub-brain regions, six whole brain tissues per group were divided into the olfactory bulb, hippocampus, cerebral cortex and cerebellum and stored in −65 °C for later use.

2.3. Nissl staining of murine brain sections

Coronal sections (about 50 μm) were cut through the whole brain in a cryostat, and at least seven sections were collected at the hippocampal position of interest. Three to four sections were used for Nissl staining with cresyl violet. Two adjacent sections were used for detection of activation of astrocytes by the method employing GFAP immunohistochemical staining. The other two sections were put on polycarbonate membrane for scanning distribution of titanium. Thus, the relationship between Ti levels and pathological changes in the corresponding area of brain can be compared.

The pathological change of neurons after Nissl staining was observed under a light microscope (Nikon U-III Multi-point Sensor System, USA) by an independent pathologist. For the counting of neurons, the number of surviving neurons in the hippocampus (in particular CA1 cell layer) from three to four sections per animal was counted by a blinded observer using light microscopy. Only whole neurons with visible nucleus were counted. The data were expressed as surviving cell number per square mm.

2.4. Scanning titanium distribution in brain sections

The scanning analysis of titanium was carried out at 4W1B platform of Beijing Synchrotron Radiation Facility (BSRF) with the photon energy of 2.2 GeV. The current intensity was about 50–100 mA. The combination of microbeam scanning and spectral analysis technique of synchrotron radiation X-ray fluorescence analysis (SRXRF) directly give the spatial distribution of interested elements (Wang et al., 2007a).

2.5. Determination of titanium content in whole brain and sub-brain regions

The olfactory bulb, hippocampus, cerebral cortex and cerebellum were digested using concentrated nitric acid (ultrapure grade) overnight (Wang et al., 2007b). Inductively coupled plasma–mass spectrometry (ICP–MS, Thermo Elemental X7, Thermo Electron Co.) was used to analyze the titanium concentration in each sample quantitatively. The detection limit of titanium was 0.074 ng/ml.

2.6. GFAP quantification

Glial fibrillary acidic protein was also quantitatively determined using the method of enzyme linked immunosorbent assay (ELISA). The assays were performed strictly according to the manufacturer's instructions. The detection limit is 1 pg/ml for GFAP. Briefly, a monoclonal anti-mouse GFAP antibody (1:200 times; BD Biosciences) has been pre-coated onto an ELISA microplate. Standards and samples are diluted in PBS and pipetted into the wells and any GFAP present is bound by the immobilized antibody. Polyclonal HRP-conjugated goat anti-rabbit Ig Ab (1:1000; BD Biosciences) was used to measure the fixation of primary Abs.

2.7. Immunohistochemistry method

Immunochemistry procedures of GFAP in hippocampus and cerebral cortex were also conducted using a commercial kit according to the manufacturer's instructions. The brains embedded in paraffin were coronary sectioned with a microtome for 4 μm thickness and mounted on the glass slides. The immunostaining was performed at room temperature. The sections were air-dried and dewaxed in dimethylbenzene, then dehydrated in a graded series of ethanol and washed with distilled water for 5 min and phosphate buffer saline (PBS, pH 7.4) three for 5 min. The sections were incubated with 0.3% Triton X-100 for 30 min at 37 °C and washed with PBS three times, then heat induced epitope retrieval method was applied for antigen retrieval using citrate buffer (0.01 mol/L, pH 6.0) for 10 min at 90 °C. After they were cooled to room temperature, the sections were incubated in a 3% H_2O_2 solution for 15 min and washed with PBS three times. After blocking with goat serum for 1 h, the sections were incubated with rabbit polyclonal antibody against GFAP (1:100, Boster Bioengineering Co. Ltd. Wuhan) overnight, and washed with PBS three times. The sections were then incubated with biotinylated anti-rabbit IgY (1:200) for 1 h, washed with PBS three times, and then incubated with the complex of avidin and biotinylated horseradish peroxidase for 1 h. After rinsing with PBS three times, the immunoreactive product was detected by using diaminobenzadine. Following the enzymatic incubation step, sections were washed with distilled water and dehydrated in a graded series of ethanol and cleared in dimethylbenzene, coverslipped using DPX. The expression level of GFAP in brain sections were observed by the microscopy (OLYMPUS IX71, Japan) and counted by an independent pathologist after immunohistochemical staining.

2.8. Assay of enzymatic activities

The brain tissues were weighed, homogenized and transferred into a centrifuge tube. After adding the 1:4 (W/V) volume of cold 0.1 mol/L phosphate buffer (0.1 mol/L Na_2HPO_4, 0.1 mol/L KH_2PO_4, 0.1 mmol/L PMSF, pH 7.4), the mixtures were homogenized by a ultrasonic cell disruptor (Sonics vibra cell, VCX105) for 8 s 4× times at 4 °C. An aliquot of 200–300 μl homogenates was taken out to determine the titanium content. The remainder homogenates were centrifuged at 14,000 × g for 5 min in 4 °C, collecting the supernatants for assaying some enzymes.

The activities of glutathione peroxidase (GSH-Px), glutathione S-transferase (GST), superoxidase dismutase (SOD), catalase (CAT), the levels of reduced glutathione (GSH) and lipid peroxidation (marked as malondiadehyde (MDA)) in the brain homogenate were examined as described previously (Chen et al., 2006; Wang et al., 2006). The activity of AChE was measured according to the method developed by Ellman et al. (1961), which employed acetythiocholine iodine (ATChI) as a

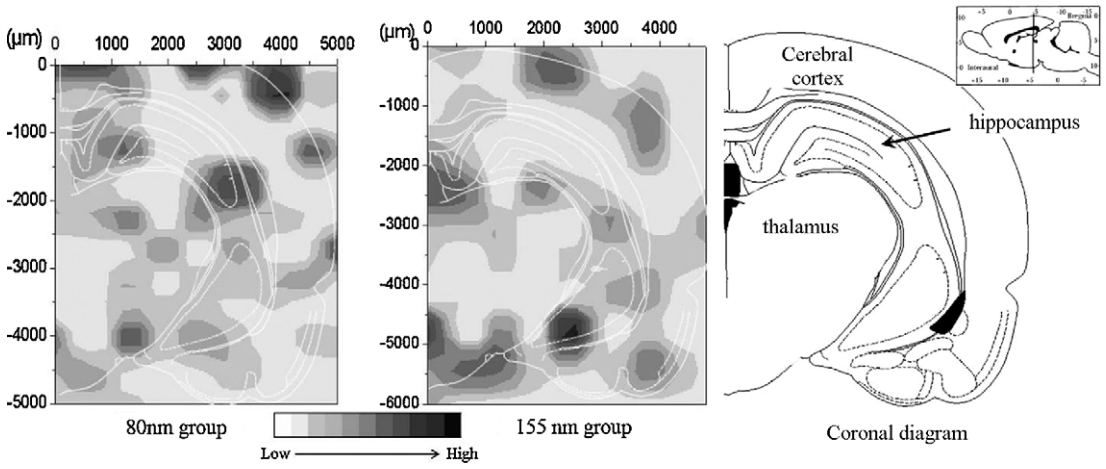

Fig. 2. SRXRF mapping of Ti-element distribution in the brain sections at 30 days after intranasal instillation of the different-sized TiO_2 particles. In the control mice, the Ti contents are lower than the detection limit of SRXRF and the mapping is not available.

synthetic substrate. One unit is defined as the amounts of ATChI broken down by AChE per 6 min. Results were expressed as one unit per milligram protein. Protein concentrations were determined according to the Bradford's method (1976).

2.9. Protein carbonyl assay

Protein carbonyls were quantified by spectrophotometric measurement of 2,4-dinitrophenylhydrazine (DNPH) derivatives ($\varepsilon_{370\,nm} = 22{,}000\,M^{-1}\,cm^{-1}$) as described by Levine et al. (1990). DNA in brain supernatant was removed by 20% streptomycin. Proteins in DNA free supernatant were derivatived by 10 mM DNPH dissolved in 2 mol/L hydrochloric acid. The mixture were precipitated and pelleted by 20% trichloroacetic acid (TCA) and centrifuged at $14{,}000 \times g$ for 10 min. The pellet was washed at least three times with ethanol/ethyl acetate (1:1) mixture to remove the unreacted DNPH. Then the pellet was dissolved in guanidine hydrochloride/dithiothreitol at 37 °C and the absorbance of aliquots was read in a spectrophotometer (SpectraMax M2, Molecular Devices Co., USA) at 370 nm.

2.10. Determination of glutamic acid and NO

The content of Glu was determined spectrophotometrically by detecting the changes of absorbency at 340 nm when the coenzyme NAD^+ was oxidized to NADH with the glutamic acid being hydrolyzed to α-ketoglutarate by glutamate dehydrogenase. NO in the homogenate was measured using the method of nitric reductase (Green et al., 1982).

2.11. Statistical analysis

Results were expressed as mean ± standard deviation (S.D.). All the statistical analysis was implemented using SPSS 10.0 (SPSS Inc., Chicago, USA). A one-way analysis of variance (ANOVA) following a post hoc Tukey's multiple comparison test is used to compare all groups of animals in the study. $p < 0.05$ was considered as the statistical significance.

3. Results

First, the micro-distribution of Ti in the brain sections was qualitatively measured using microbeam mapping technique of SRXRF. The position and coronal diagram of brain sections were shown in Fig. 2. As the size for X-ray beam was 60 μm × 80 μm, the absolute detection limit of SRXRF is 10^{-12} to 10^{-15} g. We found that titanium was mainly accumulated in the cerebral cortex, thalamus and hippocampus, especially in the CA1 and CA3 regions of hippocampus (Fig. 2) after exposure to the different-sized TiO_2 particles.

Then, the contents of Ti in the whole brain and sub-brain regions (including olfactory bulb, cerebral cortex, hippocampus and cerebellum) were quantitatively analyzed using ICP–MS. After exposure to 80 and 155 nm TiO_2 nanoparticles for 30 days, the significant increased Ti content in the whole brain of mice was detected (Fig. 3). However, in the 80 and 155 nm TiO_2 exposed mice, olfactory bulb and hippocampus are two major target sites for Ti. The highest content was observed in the hippocampus, while, the lowest Ti content was found in the cerebral cortex of brain.

To examine possible defects in whole brain, in particular, hippocampus, the Nissl staining was used to perform quantitative analysis of neuron number and immunohistochemistry staining provided the information of the distribution of GFAP-positive glial cells. The Nissl staining method is used for the detection of Nissl body in the cytoplasm of neurons and for identifying the basic neuronal structure in brain. The Nissl body will be stained purple-blue. By Nissl staining, no apparent structural difference was found in cerebral cortex and cerebellum between exposed and normal mice. However, to our surprise, we found that TiO_2-exposed mice were found to have enlarged and elongated pyramidal cell soma (Fig. 4), and for this reason, the stratum pyramidale was irregular in appearance (Fig. 4C and D). Staining became light, and the number of Nissl body decreased or disappeared. There is obviously dispersed arrangement of neurons in the CA1 region of hippocampus after exposure to the different-sized TiO_2 nanoparticles. On the other hand, the cell number was obviously changed in the hippocampal sections of exposed mice compared to control (Fig. 4E). Comparison of cell numbers in the stratum pyramidale of CA1 region also indicated the drastic neuronal loss in the mice treated with different TiO_2 nanoparticle. There are 30% and 25% cell lost in 80 and 155 nm TiO_2 exposed groups, respectively. Accordingly, the higher lesions

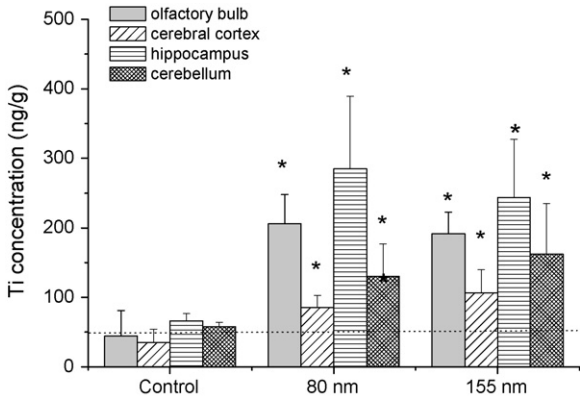

Fig. 3. Titanium content in the whole brain (dash line) and olfactory bulb, cerebral cortex, hippocampus and cerebellum of murine brain ($n = 6$) at 30 days after intranasal instillation of the different-sized TiO_2. Data are expressed as ng Ti per gram fresh tissue.

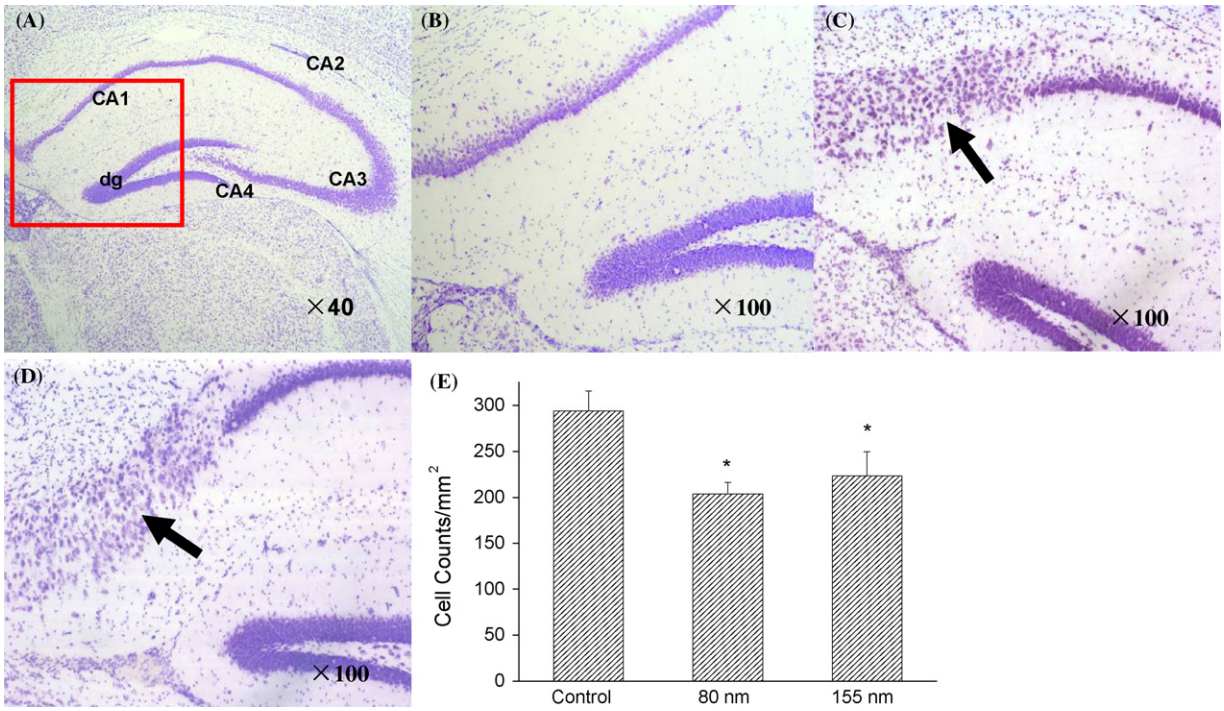

Fig. 4. Morphological changes of neurons in the Nissl stained brain tissue sections of (A&B) control group, (C) 80 nm group and (D) 155 nm group. Note that apparently scattered Nissl body, large cell somata (arrows) and an irregular appearance were found especially in the CA1 region of hippocampus in the exposed mice. Image magnification: 100× (B–D); 40× (A). E represents the comparison of cell numbers in the CA1 region of the hippocampus (number/mm^2) of mice 30 days after treatment with different TiO_2 nanoparticle.

on the neural cells are in a good agreement with the data that high accumulation of Ti in the hippocampus, in particular in CA1 region obtained by SRXRF mapping and ICP–MS.The quantitative analysis revealed an significant increase of GFAP levels in the hippocampus in the mice exposed to TiO_2 nanoparticles, in particular, the GFAP content in the 155 nm TiO_2 group was almost 2.5 times of the control (Fig. 5).

Fig. 6 (200×) reveals that there are some increases in the intensity of staining for GFAP in the nanoparticles-treated mice, especially in the CA4 region of hippocampus (Fig. 6A and B). However, we did not find any obvious difference in the cerebral cortex between control and exposed group. GFAP is best viewed as a biomarker of early biological effects, which indicates the activation of astrocytes. The number of GFAP-positive astrocytes significantly increased in the hippocampal sections of exposed mice and there is about 38% increase compared to control (Fig. 6C). However, it is difficult to recognize the variations in the morphology and appearance of the astrocytes at this magnification.

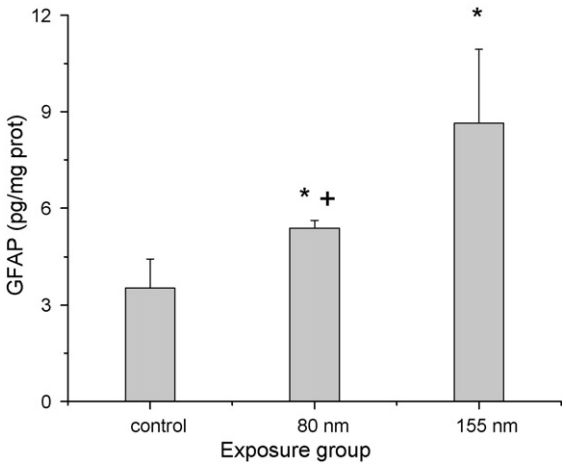

Fig. 5. Levels of GFAP protein in the hippocampus of marine brain ($n = 6$) intranasally instilled 80 and 155 nm TiO_2 particles for 30 days. *Represents $p < 0.05$ compared to the control group, +represents $p < 0.05$ compared to the 155 nmTiO_2 group.

Subsequently, the protein content and antioxidative enzymes in brain tissues were examined at 30 days after intranasal instillation of the different-sized TiO_2 nanoparticles (Table 2). Comparing with the control, there are no obvious change found for the protein and GSH contents, GSH-Px and GST activities in the experimental groups. However, CAT activity increased significantly ($p < 0.05$) in the 80 and 155 nm groups, and SOD activity decreased significantly ($p < 0.05$) in the 155 nm group. Furthermore, lipid peroxidation marked as MDA content are significantly upregulated ($p < 0.05$) in the 80 and 155 nm groups (Fig. 7). The soluble protein carbonyl content in murine brain showed a significant increase ($p < 0.05$) in all experimental groups (Fig. 7). All of these data indicate that intranasal instilled TiO_2 nanoparticles could influence the balance of endogenous antioxidative system in murine brain.

The significantly upregulated activities of AChE in the murine brain were observed after exposure to different-sized TiO_2 particles (Fig. 8). Glutamic acid, the most abundant excitatory neurotransmitter in the nervous system, its concentrations in the brain increase significantly ($p < 0.05$) after intranasal instillation of the different-sized TiO_2 particles (Fig. 9). The percentages of increased Glu are 26.9% and 30.9% in the 80 and 155 nm groups, respectively (Fig. 9). NO levels in the 80 and 155 nm groups also increase significantly comparing with the control (Fig. 9). However, NO in whole brain homogenates would reflect NO produced for neurotransmission, but also reflect NO produced by inflammatory responses initiated by TiO_2 nanoparticles, a potentially important observation.

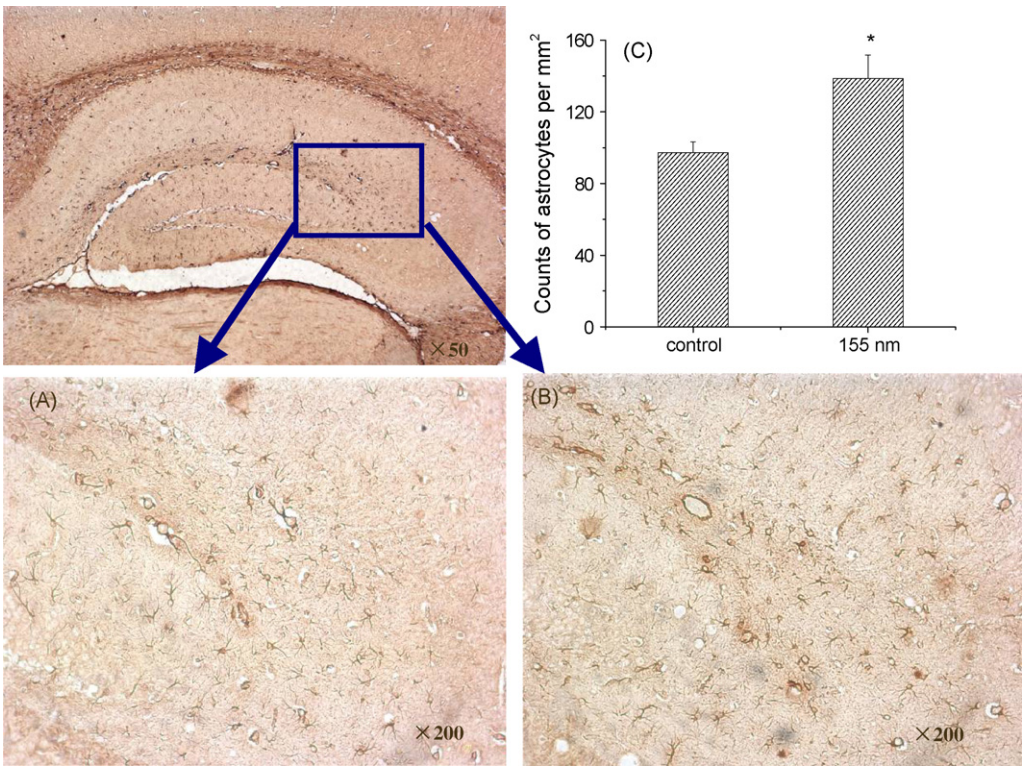

Fig. 6. Immunohistochemical staining of GFAP in hippocampus of mice after intranasally instilled TiO_2 nanoparticles for 30 days. The cartoon-like illustration of the region is used to indicate the position where A and B correspond to in the hippocampus, i.e. CA4 region. (A) Control group (200×); (B) 155 nm group (200×); (C) cell counting analysis of GFAP-positive astrocytes in the CA4 region of the hippocampus (number/mm^2).

Table 2
Protein content and redox status in female murine brain at 30 days after intranasal instillation of the different-sized TiO_2 ($n = 6$).

Groups	Body weight (g)	Protein (mg/ml)	GSH-Px (U/mg prot)	GSH (mg/g prot)	GST (U/mg prot)	CAT (U/mg prot)	SOD (U/mg prot)
Control	27.2 ± 2.2	0.89 ± 0.09	1.33 ± 0.12	23.11 ± 2.78	36.11 ± 4.12	2.10 ± 0.49	97.51 ± 8.90
80 nm	27.6 ± 1.9	0.85 ± 0.11	1.34 ± 0.12	22.36 ± 3.06	36.35 ± 3.24	3.15 ± 0.60[a]	90.20 ± 13.34
155 nm	28.1 ± 0.9	0.85 ± 0.10	1.31 ± 0.36	22.71 ± 4.04	35.09 ± 5.25	3.85 ± 0.38[a]	80.58 ± 10.14[a]

[a] $p < 0.05$ significantly different from the control group.

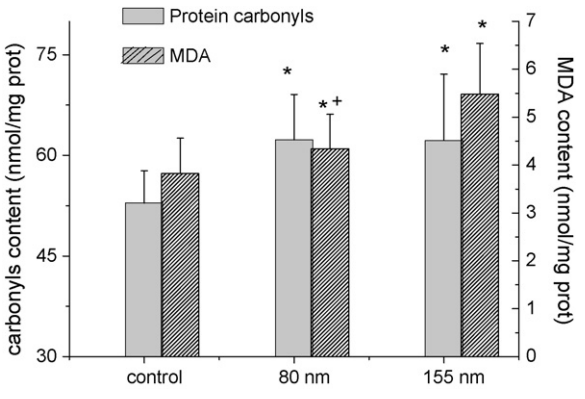

Fig. 7. Protein carbonyls and MDA contents in whole murine brain ($n = 6$) at 30 days after intranasal instillation of the different-sized TiO_2. Carbonyl levels for protein oxidation were measured by DNPH assay in soluble proteins from the murine brain. MDA contents for lipid peroxidation in the brain were examined by thiobarbituric acid reactive substances using 1,1,3,3-tetraethoxypropane (TEP) as a standard. $^*p < 0.05$ significantly different from the control group; $^+p < 0.05$ significantly different from the 155 nm group.

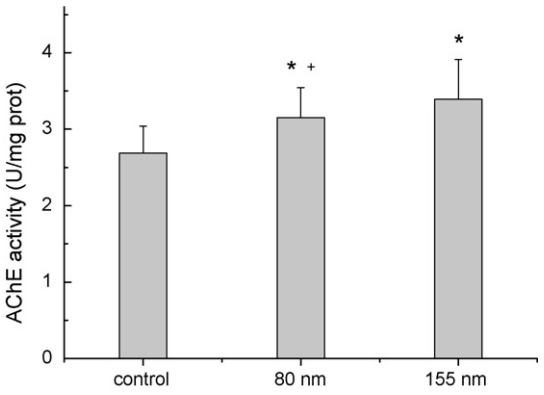

Fig. 8. AChE activities in whole murine brain ($n = 6$) at 30 days after intranasal instillation of the different-sized TiO_2. $^*p < 0.05$ significantly different from the control group; $^+p < 0.05$ significantly different from the 155 nm group.

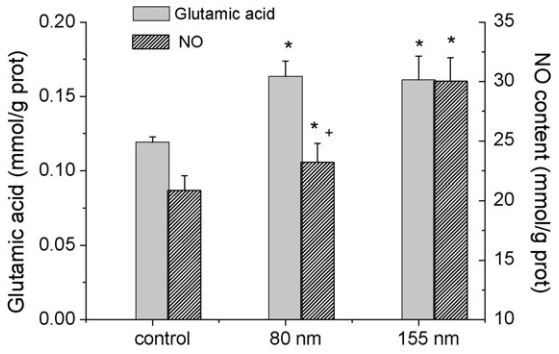

Fig. 9. Glutamic acid and NO concentrations in whole murine brain ($n=6$) at 30 days after intranasal instillation of the different-sized TiO_2. $^{*}p<0.05$ significantly different from the control group; $^{+}p<0.05$ significantly different from the 155 nm group.

4. Discussion

4.1. Olfactory translocation of TiO_2 particles to the central nervous system

Titanium dioxide belong to the group of poorly soluble, low-toxicity particles from acute toxicity evaluation (Wang et al., 2007a, 2007b; Warheit et al., 2007c). However, in accordance with the documents published by National Institute for Occupational Safety and Health (NIOSH), titanium dioxide is considered as a potential occupational carcinogen, which is defined by the Occupational Safety and Health Act or Adiministration (OSHA) carcinogen policy (Baan et al., 2006). Overall, the results from rodent cancer studies with TiO_2 were determined to provide sufficient evidence to be labeled as possibly carcinogenic to humans (Group 2B) (Baan et al., 2006). The current OSHA permissible exposure limits (PEL) are 15 mg/m^3 TWA and the immediately dangerous to life or health concentrations (IDLHs) is 7500 mg/m^3. As a man inhales air of 15–20 m^3 per day, taking the higher level 20 m^3 per day, the calculated exposure levels of a 50-kg individual are 6 and 3000 mg/kg for PEL and IDLH, respectively. The median cumulative exposure of workers was 1.98 mg/m^3 years (interquartile range 0.26–6.88 mg/m^3 years) (Boffetta et al., 2004). The median time-weighted average exposure of workers (cumulative exposure index divided by duration of exposure) was estimated to be 10 mg/m^3 at 11 European and 4 US TiO_2 manufacturing plants. Fortunately, there was no suggestion of any carcinogenic effect associated with workplace exposure to TiO_2. Thereafter, in vivo the toxicology studies exposed rats, mice and hamsters to pigment-grade TiO_2 (PG-TiO_2, 0, 10, 50 and 250 mg/m^3) or ultrafine TiO_2 (UF-TiO_2, 0, 0.5, 2 and 10 mg/m^3) for 90 days and the lung burdens and tissue responses were evaluated at the end of the exposure period and for up to 1 year post- exposure (Hext et al., 2005). At high lung particle burdens, rats showed a marked progression of histopathological lesions throughout the post-exposure period while mice and hamsters showed minimal initial lesions with recovery apparent during the post-exposure period. Considering these previous studies, our dose designed for the experiment was 500 μg per mice every other day. Thus, the dose is between them, higher than the PEL and lower than IDLH. We chose this dose level because we aimed to know the neurotoxicity response of TiO_2 nanoparticles under a higher exposure level, in order to provide some useful information for occupational exposure.

In this study, the experimental results show clear evidences that the intranasal instilled TiO_2 particles could be easily translocated into the cerebral cortex, thalamus, and CA1 and CA3 region of hippocampus in murine brain (Fig. 2) via the olfactory bulb (Wang et al., 2007a). The significantly increased Ti contents in the hippocampus (Fig. 3) result in the obviously irregular arrangement and loss of neurons in the hippocampus (Fig. 4). The intranasal instilled TiO_2 nanoparticles have the probability to access the CNS and ganglia along the axons and dendrites of neurons through the olfactory tract and mainly accumulated in the hippocampus. Previously, De Lorenzo (1970) had reported that the intranasally instilled silver-coated colloidal gold particles (50 nm) were translocated along the axons of the olfactory nerves to the olfactory bulbs in squirrel monkeys. Recently, there have been increasing reports that nano-sized component of particulate matters (PM) can reach the brain and may be associated with neurodegenerative diseases (Block et al., 2004; Peters et al., 2006). Oberdörster et al. (2004) reported that nanoparticles may be taken up directly to the brain from olfactory epithelium to the various part of rat brain via the olfactory nerves. A recent study showed inhaled ultrafine Manganese Oxide particles can be translocated to the central nervous system through olfactory neuronal pathway (Elder et al., 2006). Mn concentrations in the olfactory bulb increased 3.5-fold, whereas lung Mn concentrations doubled; there were also increases in striatum, frontal cortex, and cerebellum. Our results on TiO_2 nanoparticles show similar trends. The higher titanium contents in the brain tissues than lung tissues imply that the translocation and deposition of nanoparticles through intranasal instilling pathway is different from the other routes such as intratracheal inhalation or intratracheal instillation (Wang et al., in press-a). The time-dependent translocation also indicated the hippocampus was the major target of the instilled nanoparticles (Wang et al., 2008b). Intranasal instillation of either rutile or anatase TiO_2 nanoparticles produced the sustained accumulation in brain tissues especially deposit in the hippocampus during whole exposure process, which indicate that the TiO_2 nanoparticles can enter into the brain via the olfactory bulb (Wang et al., 2008b).

4.2. Potential damage on the hippocampus of exposed mice

In this study, we show that when they reach the olfactory bulbs and brains TiO_2 nanoparticles have the potential to cause oxidative stress and lesion to neural cells. After TiO_2 nanoparticles exposure, apparently scattered Nissl body, large cell somata (arrows) and an irregular appearance were found especially in the CA1 region (Fig. 4) and dentate gyrus (data not shown) of hippocampus in the exposed mice. It is well-known that the hippocampus plays a key role in learn and memory and spatial navigation. Our findings showed that the highly accumulated Ti in brain, especially in the hippocampus, could result in the morphological changes of neurons.

Increasing evidence suggests that astrocytes play an active role in CNS function by influencing or even directing the neuronal activities. GFAP is involved in many cellular functioning processes, such as cell structure and movement, cell communication, and the functioning of the blood–brain barrier. It is reported to increase dramatically in response to acute infection or neurodegeneration (Johnston-Wilson et al., 2000). In this study, the significantly higher expression of GFAP in the brain of mice was recorded (Figs. 5 and 6). The change together with the excess release of Glu and NO and increased AChE activity in the brain suggest that astrocytes might be the potential target of inhaled TiO_2 nanoparticles, but the further study should be investigated. Similarly, Elder et al. (2006) found inhaled ultrafine manganese oxide particles can increase expression of tumor necrosis factor-α mRNA (~8-fold) and protein (~30-fold), and GFAP mRNA in olfactory bulb after 11 days of exposure. In order to confirm whether some physiological lesions would occur associating with the translocation of intranasal instilled TiO_2 to the brain, we further discussed the influences of TiO_2 particles on redox status and metabolism of neurochemicals.

4.3. Oxidative damage in murine brain induced by TiO_2 particles

In the central nervous system, polyunsaturated fatty acids (PUFA) are present in large quantities, play a major role in the brain structure and represent an environmental factor able to act on the brain functioning. But, PUFA are easy to be invaded by ROS and cause impairment of cellular function (Matés, 2000). In this study, lipid peroxidation and oxidized protein (Fig. 7) coexisted in the brain and further the increased CAT and decreased SOD activity were observed when mice were exposed to TiO_2 particles, which demonstrated that the oxidative stress was greatly regulated in murine brain. Generally, TiO_2 may produce ROS and induce oxidative stress (Xia et al., 2006; Nel, 2005) due to their high reactivity. In addition, once TiO_2 was translocated into the brain, the macrophages in brain such as monocytes, neutrophils and microglia could release oxygen radicals (Colton and Gilbert, 1987) as well as phagocytizing these particles. Therefore, the synthesis of some enzymes was influenced and the balance of oxidative/antioxidative system in brain was disrupted, resulting in the lipid peroxidation and protein oxidation. Nanoparticles (TiO_2 or gold particles) are no longer freely distributed in the cytoplasm after internalized by cells but are preferentially located in mitochondria (De Lorenzo, 1970). When the mitochondria are invaded by these nanoparticles (Long et al., 2006), they possibly produce ROS and interfere with antioxidant defenses. Our time-course study of activities of GSH-Px, GST and SOD and GSH level showed that there were significant changes at 10th day post-exposure and then they were recovered to the normal level. Only MDA contents showed a consistent elevation with the prolonged exposure (Wang et al., 2008b)

4.4. Influence on metabolism of neurochemicals

Recently, there has been increasing concern that nano-sized particulate matter can be translocated into the brain and may be associated with neurodegenerative diseases. Translocating inhaled Mn oxide nanoparticles to the central nervous system can result in inflammatory changes (Elder et al., 2006; Henriksson and Tjälve, 2000). While we are preparing the manuscript, Tin-Tin-Win-Shwe et al. (2008) also showed that a single intranasal instillation of nano-sized carbon black (14 nm) can modulate the extracellular amino acid neurotransmitter levels and increase proinflammatory cytokine IL-1 β mRNA expressions synergistically in a mouse olfactory bulb within 12 h.

In the brain, the enormous content of neuronal connections and intricate mechanisms for memory encoding are the target of ROS. Butler and Bahr (2006) reviewed that oxidative stress are related with the abnormal neuronal activity, especially excitotoxicity. Acetylcholine is usually, but not always, an excitatory neurotransmitter in contrast to the monoamine neurotransmitters and synthesized in cholinergic neurons. It was hydrolyzed by AChE into the inactive metabolites choline and acetate in the synaptic cleft. In this study, the significant increased AChE activity implied that the motive nerves were activated and influenced the acetylcholine content. Another excitatory neurotransmitter-Glu, the major "workhorse" neurotransmitter of brain, was detected after TiO_2 nanoparticles entering into the murine brain (Fig. 9). From another aspect, excitotoxicity leads to ROS production in turn (Butler and Bahr, 2006). The binding of Glu and NMDA receptors can disrupt calcium homeostasis (Ca^{2+} influx) and activate calcium-dependent protease, i.e. nitric oxide synthase (NOS) in the hippocampus, causing the over production of NO in the brain of mice exposed to different-sized TiO_2 particles (Fig. 9). NO plays dual function as a free radical and signal molecule of neurotransmitter in organism. Because of the existence of ROS in murine brain after intranasal instilling TiO_2 particles, NO could be oxidized to peroxinitrite ($ONOO^-$) radical to cause the damaged neurons, as found in the pathological observations (Fig. 4).

In this study, it should be noted that the two crystal phases of the TiO_2 particle tested, i.e. rutile and anatase were selected to research their abilities of translocation into the murine brain after intranasal instillation and their neurotoxicological effects. From all results, the ability and deposition in different brain regions are almost same; however, some findings indicate anatase TiO_2 nanoparticles exhibit greater concern. The GFAP expression, MDA and NO levels and AChE activities are much higher in the 155 nm anatase TiO_2 exposed mice, which may be contributed to the nano-TiO_2 particles in the anatase crystal phase with a superior photocatalyst to the rutile particle types. Warheit et al. (2005,2007a, 2007b) also revealed a similar result that TiO_2 induced transient pulmonary toxicity was not dependent upon particle size and surface area and showed some relationship to their existing shapes i.e. TiO_2 rods and dots.

To our knowledge, this is the first time showing that the intranasal instilled nanoparticles lead to the injury of murine brain and further influence the metabolism of neurochemicals. Oxidative stress has been suggested as the most appealing paradigm for discriminating the adverse effects of different nanoparticles at the cellular and molecular levels (Stone and Donaldson, 2006), which was further demonstrated in this study. Furthermore, we found that the imbalance of antioxidative defense systems could impair the metabolism of neurochemicals. Our findings imply that the regulation of both ROS and signaling molecules should be involved in the framework of nanotoxicology, which, no doubt, needs further studies.

In conclusion, the intranasal instilled TiO_2 nanoparticles caused the obvious scattered Nissl body, large cell somata and an irregular appearance of neurons in the CA1 region of hippocampus, which is in a good agreement with Ti micro-distribution determined by SRXRF and higher Ti contents determined by ICP–MS. Deposition of TiO_2 nanoparticles in brain significantly increased the lipid peroxidation and protein oxidation in the exposed mice and also induced other specific neurochemicals. In addition, nano-TiO_2 particles in the anatase crystal phase induce higher lesion. Results imply that the translocation of TiO_2 particles into the brain may affect brain functions and specific target to astrocytes, in which physiological significance is required to be studied in next step. The present results suggest that the techniques for occupational protection should be developed for workers at workplace.

Conflict of interest

None.

Acknowledgments

We thank financial support from the National Science Foundation for Distinguished Young Scholars (10525524), the MOST 973 programs (2006CB705603), the National Natural Science Foundation of China (20751001 and 10490180), and the Knowledge Innovation Program of Chinese Academy of Sciences.

References

Baan, R., Straif, K., Grosse, Y., Secretan, B., Ghissassi, F.E., Cogliano, V., 2006. Carcinogenicity of carbon black, titanium dioxide, and talc. Lancet Oncol. 7 (4), 295–296.

Bermudez, E., Mangum, J.B., Asgharian, B., Wong, B.A., Reverdy, E.E., Janszen, D.B., Hext, P.M., Warheit, D.B., Everitt, J.I., 2002. Long-term pulmonary responses of three laboratory rodent species to subchronic inhalation of pigmentary titanium dioxide particles. Toxicol. Sci. 70, 86–97.

Bermudez, E., Mangum, J.B., Wong, B.A., Asgharian, B., Hext, P.M., Warheit, D.B., Everitt, J.I., 2004. Pulmonary responses of mice, rats, and hamsters to subchronic inhalation of ultrafine titanium dioxide particles. Toxicol. Sci. 77, 347–357.

Block, M.L., Wu, X., Pei, Z., Li, G., Wang, T., Qin, L., Wilson, B., Yang, J., Hong, J.S., Veronesi, B., 2004. Nanometer size diesel exhaust particles are selectively toxic to dopaminergic neurons: the role of microglia, phagocytosis, and NADPH oxidase. FASEB J. 18, 1618–1620.

Boffetta, P., Soutar, A., Cherrie, J.W., Granath, F., Anderson, A., Anttila, A., Blettner, M., Gaborieau, V., Klug, S.J., Langard, S., Luce, D., Merletti, F., Miller, B., Mirabelli, D., Pukkala, E., Adami, H.O., Weiderpass, E., 2004. Mortality among workers employed in the titanium dioxide production industry in Europe. Cancer Causes Control 15, 697–706.

Bradford, M.M., 1976. A rapid and sensitive method for the quantitation of microgram quantities of protein utilizing the principle of protein–dye binding. Anal. Biochem. 72, 248–254.

Butler, D., Bahr, B.A., 2006. Oxidative stress and lysosomes: CNS-related consequences and implications for lysosomal enhancement strategies and induction of autophagy. Antioxid. Redox Signal 8, 185–196.

Chen, C.Y., Yu, H.W., Zhao, J.J., Li, B., Qu, L.Y., Liu, S.P., Zhang, P.Q., Chai, Z.F., 2006. The roles of serum selenium and selenoproteins upon mercury toxicity in environmental and occupational exposure. Environ. Health Perspect. 114 (2), 297–301.

Colton, C.A., Gilbert, D.L., 1987. Production of superoxide anions by a CNS macrophage, the microglia. FEBS Lett. 223, 284–288.

Colvin, V.L., 2003. The potential environmental impact of engineered nanomaterials. Nat. Biotechnol. 21 (10), 1166–1170.

De Lorenzo, A.J., 1970. The olfactory neuron and the blood–brain barrier. In: Wolstenholme, G., Knight, J. (Eds.), Taste and Smell in Vertebrates London. J&A Churchill, pp. 151–176.

Donaldson, K., Stone, V., Tran, C.L., Kreyling, W., Borm, P.J.A., 2004. Nanotoxicology: a new frontier in particle toxicology relevant to both the workplace and general environment and to consumer safety. Occup. Environ. Med. 61, 727–728.

Elder, A., Gelein, R., Silva, V., Feikert, T., Opanashuk, L., Carter, J., Potter, R., Maynard, A., Ito, Y., Finkelstein, J., Oberdörster, G., 2006. Translocation of inhaled ultrafine manganese oxide particles to the central nervous system. Environ. Health Perspect. 114, 1172–1178.

Ellman, G.L., Courtney, K.D., Andres, V., Featherstone, R.M., 1961. A new and rapid colorimetric determination of acetylcholinesterase activity. Biochem. Pharmacol. 7, 88–95.

Green, L.C., Wagner, D.A., Glogowski, J., Skipper, P.L., Wishnok, J.S., Tannenbaum, S.R., 1982. Analysis of nitrate, nitrite, and [^{14}N]nitrite in biological fluids. Anal. Biochem. 126, 131–138.

Henriksson, J., Tjälve, H., 2000. Manganese taken up into the CNS via the olfactory pathway in rats affects astrocytes. Toxicol. Sci. 55, 392–398.

Hext, P.M., Tomenson, J.A., Thompson, P., 2005. Titanium dioxide: inhalation toxicology and epidemiology. Ann. Occup. Hyg. 49 (6), 461–472.

Johnston-Wilson, N.L., Sims, C.D., Hofmann, J.P., Anderson, L., Shore, A.D., Torrey, E.F., Yolken, R.H., 2000. Disease-specific alterations in frontal cortex brain proteins in schizophrenia, bipolar disorder, and major depressive disorder. The Stanley Neuropathology Consortium. Mol. Psychiatry 5 (2), 142–149.

Levine, R.L., Garland, D., Oliver, C.N., Amici, A., Climent, I., Lenz, A.G., Ahn, B.W., Shaltiel, S., Stadtman, E.R., 1990. Determination of carbonyl contents in oxidatively modified proteins. Methods Enzymol. 186, 464–478.

Long, T.C., Saleh, N., Tilton, R.D., Lowry, G., Veronesi, B., 2006. Titanium dioxide (P25) produces reactive oxygen species in immortalized brain microglia (BV2): implications for nanoparticle neurotoxicity. Environ. Sci. Technol. 40, 4346–4352.

Matés, J.M., 2000. Effects of antioxidant enzymes in the molecular control of reactive oxygen species toxicology. Toxicology 153, 83–104.

Nel, A.E., 2005. Air pollution-related illness: effects of particles. Science 308, 804–806.

Nel, A., Xia, T., Mädler, L., Li, N., 2006. Toxic potential of materials at the nanolevel. Science 311 (3), 622–627.

Normandin, L., Beaupre, L.A., Salehi, F., St.-Pierre, A., Kennedy, G., Mergler, D., Butterworth, R.E., Philippe, S., Zayed, J., 2004. Manganese distribution in the brain and neurobehavioral changes following inhalation exposure of rats to three chemical forms of manganese. Neuro. Toxicol. 25 (3), 433–441.

Oberdörster, E., 2004. Manufactured nanomaterials (Fullerenes, C60) induce oxidative stress in the brain of juvenile largemouth bass. Environ. Health Perspect. 112 (10), 1058–1062.

Oberdörster, G., Ferin, J., Gelein, R., Soderholm, S.C., Finkelstein, J., 1992. Role of the alveolar macrophage in lung injury: studies with ultrafine particles. Environ. Health Perspect. 97, 193–199.

Oberdörster, G., Oberdörster, E., Oberdörster, J., 2005. Nanotoxicology: an emerging discipline evolving from studies of ultrafine particles. Environ. Health Perspect. 113 (7), 823–839.

Oberdörster, G., Sharp, Z., Atudorei, V., Elder, A., Gelein, R., Kreyling, W., Cox, C., 2004. Translocation of inhaled ultrafine particles to the brain. Inhal. Toxicol. 16 (6–7), 437–445.

Oberdörster, G., Utell, M.J., 2002. Ultrafine particles in the urban air: to the respiratory tract and beyond? Environ. Health Perspect. 110A, 440–441.

Peters, A., Veronesi, B., Calderón-Garcidueñas, L., Gehr, P., Chen, L.C., Geiser, M., Reed, W., Rothen-Rutishauser, B.M., Schürch, S., Schulz, H., 2006. Translocation and potential neurological effects of fine and ultrafine particles a critical update. Part. Fibre Toxicol. 3, 1–13.

Rahman, Q., Lohani, M., Dopp, E., Pemsel, H., Jonas, L., Weiss, D.G., Schiffmann, D., 2002. Evidence that ultrafine titanium dioxide induces micronuclei and apoptosis in syrian hamster embryo fibroblasts. Environ. Health Perspect. 110, 797–800.

Stone, V., Donaldson, K., 2006. Nanotoxicology: signs of stress. Nat. Nanotechnol. 1, 23–24.

Tin-Tin-Win-Shwe, Mitsushima, D., Yamamoto, S., Fukushima, A., Funabashi, T., Kobayashi, T., Fujimaki, H., 2008. Changes in neurotransmitter levels and proinflammatory cytokine mRNA expression in the mice olfactory bulb following nanoparticle exposure. Toxicol. Appl. Pharmacol. 226, 192–198.

Wamer, W.G., Yin, J., Wei, R., 1997. Oxidative damage to nucleic acids photosensitized by titanium dioxide. Free Radic. Biol. Med. 23, 851–858.

Wang, J.X., Chen, C.Y., Li, B., Yu, H.W., Zhao, Y.L., Sun, J., Li, Y.F., Xing, G.M., Yuan, H., Tang, J., Chen, Z., Meng, H., Gao, Y.X., Ye, C., Chai, Z.F., Zhu, C.F., Ma, B.C., Fang, X.H., Wan, L.J., 2006. Antioxidative function and biodistribution of $[Gd@C_{82}(OH)_{22}]_n$ nanoparticles in tumor-bearing mice. Biochem. Pharmacol. 71, 872–881.

Wang, J.X., Chen, C.Y., Yu, H.W., Sun, J., Li, B., Li, Y.F., Gao, Y.X., Chai, Z.F., He, W., Huang, Y.Y., Zhao, Y.L., 2007a. Distribution of TiO_2 particles in the olfactory bulb of mice after nasal inhalation using microbeam SRXRF mapping techniques. J. Radioanal. Nucl. Chem. 272 (3), 527–531.

Wang, J.X., Zhou, G.Q., Chen, C.Y., Yu, H.W., Wang, T.C., Ma, Y.M., Jia, G., Gao, Y.X., Li, B., Sun, J., Jiao, F., Zhao, Y.L., Chai, Z.F., 2007b. Acute toxicity and biodistribution of different sized titanium dioxide particles in mice after oral administration. Toxicol. Lett. 168, 176–185.

Wang, J.X., Li, Y.F., Li, W., Chen, C.Y., Li, B., Zhao, Y.L., in press-a. Biological effect of intranasally instilled titanium dioxide nanoparticles on female mice. NANO: Brief Reports and Reviews.

Wang, J.X., Liu, Y., Jiao, F., Wang, T.C., Lao, F., Li, W., Gu, Y.Q., Li, Y.F., Ge, C.C., Zhou, G.Q., Li, B., Zhao, Y.L., Chai Z.F., Chen, C.Y., 2008b. Time-dependent translocation and potential impairment on central nervous system by intranasally instilled TiO_2 nanoparticles. Toxicology. doi:10.1016/j.tox.2008.09.014.

Warheit, D.B., Brock, W.J., Lee, K.P., Webb, T.R., Reed, K.L., 2005. Comparative pulmonary toxicity inhalation and instillation and studies with different TiO_2 particle formulations: impact of surface treatments on particle toxicity. Toxicol. Sci. 88, 514–524.

Warheit, D.B., Webb, T.R., Reed, K.L., Frerichs, S., Sayes, C.M., 2007a. Pulmonary toxicity study in rats with three forms of ultrafine-TiO_2 particles: differential responses related to surface properties. Toxicology 230, 90–104.

Warheit, D.B., Webb, T.R., Colvin, V.L., Reed, K.L., Sayes, C.M., 2007b. Pulmonary bioassay studies with nanoscale and fine-quartz particles in rats: toxicity is not dependent upon particle size but on surface characteristics. Toxicol. Sci. 95 (1), 270–280.

Warheit, D.B., Hokea, R.A., Finlaya, C., Donnera, E.M., Reeda, K.L., Sayesa, C.M., 2007c. Development of a base set of toxicity tests using ultrafine TiO_2 particles as a component of nanoparticle risk management. Toxicol. Lett. 171 (3), 99–110.

Xia, T., Kovochich, M., Brant, J., Hotze, M., Sempf, J., Oberley, T., Sioutas, C., Yeh, J., Wiesner, M.R., Nel, A.E., 2006. Comparison of the abilities of ambient and manufactured nanoparticles to induce cellular toxicity according to an oxidative stress paradigm. Nano Lett. 6 (8), 1794–1807.

Yamamoto, S., Ahmed, S., Kobayashi, T., Fujimaki, H., 2006. Effect of ultrafine carbon black particles on lipoteichoic acid-induced early pulmonary inflammation in BALB/c mice. Toxicol. Appl. Pharmacol. 213, 256–266.